

SpooF Surface Plasmon Polariton Beam Splitter

Mahdi Aghadjani, Mikhail Erementchouk, and Pinaki Mazumder, *Fellow, IEEE*

Abstract—Propagation of terahertz (THz) wave utilizing spooF surface plasmon polariton (SSPP) earned a great deal of attention due to the ability of SSPP modes to guide THz waves at very low dispersion. We present an investigation of the SSPP beam splitter, one of the key elements of many optical setups. In contrast with conventional free space implementations, in the case of the SSPP beam splitter, one can no longer disregard scattering of incoming wave back into the input channels. Thus, SSPP implementations must take into consideration both the splitting ratio and the backscattering as important parameters characterizing the beam splitter. Three different designs representing different approaches to solving the problem of the relation between these parameters are investigated. The mathematical formalism to study the dispersion diagrams is proposed. The frequency dependence of splitting ratio, scattering parameters, and backscattering for each beam splitter is investigated. Finally, by employing one of the proposed beam splitter, a controllable filter is designed and analyzed.

Index Terms—Beam splitter, dispersion relation, filter, full-field analysis, spooF surface plasmon polariton (SSPP).

I. INTRODUCTION

THE fast approaching to the communication limits in millimeter range and demand for higher bandwidth inspired researchers to exploit the underdeveloped frequency range from 0.1 to 10 THz known as the terahertz (THz) band [1]–[4]. Various THz structures have been investigated in past decade to provide the solution to constantly increasing demand for higher communication speed. Despite these efforts, this region is remaining underexploited due to the fact that most of the proposed components, such as sources and detectors, are working at lab scale and their implementation in real-world applications is still challenging [5].

There are several major hurdles in developing THz components such as high power sources working at room temperature, high sensitivity detectors, and low loss guiding structures. Recently, some structures have been proposed that can detect THz signals at a high speed [6], [7]. In the field of THz sources, resonant tunneling diodes and photoconductive antennas have been explored as the candidates that can deliver the substantial power in the THz range at room temperature [8]–[10]. In the area of guiding THz waves, Grischkowsky *et al.* used the conventional electromagnetic (EM) metallic hollow waveguides in the THz

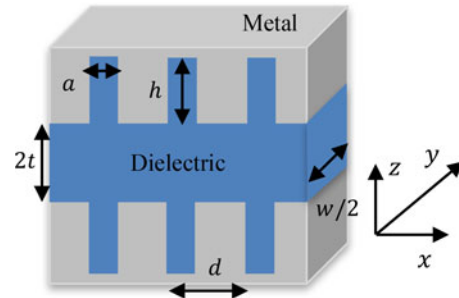


Fig. 1. Two-sided corrugated waveguide. For structures analyzed below, the typical sizes are taken to be $h = 80 \mu\text{m}$, $a = 12 \mu\text{m}$, $w = 300 \mu\text{m}$, $d = 100 \mu\text{m}$, $t = 33 \mu\text{m}$.

frequency spectrum [11], [12]. Besides this, there have been efforts to investigate and utilize structures such as subwavelength metal wires waveguide, tubes, index-guiding silicon slab waveguides or sapphire fibers, etc. [13]–[16] as candidates to guide THz waves. However, there are still some obstacles such as high metal loss, high bending loss, coupling difficulty, group velocity dispersion, and fabrication difficulty [17]. To overcome the aforementioned problems, researcher tried to apply some of the previously developed ideas from optical domain such as using surface plasmon polariton (SPP) modes and implement them at THz band. There have been significant theoretical and experimental efforts to utilize these modes in the THz frequency range (0.3–10 THz), but, because of the losses in metals at this range, the efficiency of using SPP is low [17]. The proposed method to overcome the weak guiding of SSP modes at THz frequencies is the utilization of spooF surface plasmon polariton (SSPP) waves confined to the periodically corrugated metallic structures. First by Wang and Mittleman, the possibility of having dispersion-less propagation along metallic wire surrounded by dielectric at THz frequency was shown in [18]. Later, Pendry *et al.* proposed a periodic structure containing grooves at metallic dielectric interface to support THz propagation [19]. These SSPP modes exhibit features such as field enhancement and localization. Different structures have been proposed and analyzed that are capable of guiding SSPP modes, such as doubly corrugated rectangular waveguide (DC-SSPP) (see Fig. 1), cylindrical corrugated waveguide (C-SSPP), corrugated coaxial waveguide, corrugated wires, etc. [17], [20]–[22]. Utilizing these waveguides, several components have been presented in the literatures including fast THz switches [23]–[26], analog-to-digital convertor [27], which are applicable in designing THz logic circuitry. Besides those, there are efforts to propose and design passive components using SSPP waveguides. One of the components which is the important building block of every optical setup and, therefore, is necessary in THz range is beam splitter. In general, beam splitters used in THz setup are polar-

Manuscript received October 8, 2015; revised January 29, 2016; accepted March 6, 2016. Date of publication August 31, 2016; date of current version November 1, 2016. This work was supported in part by the Air Force Office of Scientific Research, Arlington, VA, USA, under Grant FA 9550-12-1-0402, and in part by the National Science Foundation under Grant 1116040.

The authors are with the Electrical Engineering and Computer Science Department, University of Michigan, Ann Arbor, MI 48109 USA (e-mail: mahdia@umich.edu; merement@umich.edu; pinakimazum@gmail.com).

Color versions of one or more of the figures in this paper are available online at <http://ieeexplore.ieee.org>.

Digital Object Identifier 10.1109/TTHZ.2016.2599289

izing metallic grids, dielectric films, or substrate-coated beam splitters [29]–[31].

Coated dielectric beam splitters, however, introduce significant loss; for example, if the dielectric is made of alkali-halide, it shows high absorption at frequencies below 7 THz [29]. Metamaterial-based beam splitters, in turn, are mostly working at specific polarization and are not suitable for wavelength smaller than the structure's period.

This paper organized as follows: in Section II, we discuss the main properties of three different beam splitter structures. The scattering parameters are calculated in a high frequency structural simulator (HFSS) to compare and justify the analytical results. In Section III, the four-port beam splitter is discussed in the context of quantum applications, specifically from the perspective of homodyne detection, and in Section IV, the proposed structure for tunable filter is investigated.

II. THREE DIFFERENT BEAM SPLITTER DESIGNS AND THE NUMERICAL RESULTS

The main feature drastically distinguishing SSPP BS is their reduced dimensionality. As a result, there is always scattering into the state with reversed wave vector, i.e., backscattering. Moreover, one may expect that the ability to redistribute efficiently the incoming wave into the outgoing channels is related to the strong perturbation of the SSPP flow and thus should be accompanied by the strong backscattering. The importance of the intensity of backscattering depends on details of specific applications. For example, in setups employing the small number of beam splitters, backscattered signal can be completely ignored. We address this problem in more detail in the next section in the context of prospective applications in homodyne detection schemes. On the other hand, in large-scale setups backscattering may lead to significant reduction of the output signal, which may pose the challenging obstacle. This leads to the problem of rather finding an optimal design in terms of the tradeoff between the splitting efficiency and the intensity of backscattering as is dictated by the specific application. We analyze three implementations of the SSPP BS shown in Fig. 2, which illustrates different approaches to the problem of SSPP splitting.

Transport of THz waves through the SSPP mode in double corrugated waveguide (see Fig. 2) with subwavelength dimensions has been analyzed in detail in the previous publications [21]. These results are directly applicable for the analysis of one- and two-connector (TC) beams splitters, but require a generalization in order to deal with the beam splitter design based on coupling through shared grooves. The generalization is based on applying the transfer matrix formalism for finding the spatial distribution of the EM field along the z -direction. The closed form of the transfer matrices can be found, as will be elaborated below, keeping the lowest frequency contributions, which is justified for the low frequency part of the spectrum.

As well as in [21], we consider $E_y = 0$ polarization. In this case instead of the full vectors of the electric and magnetic fields, it is sufficient to keep track of E_x , B_y , and if the waveguide contains layers with different dielectric functions, E_z components.

Then, the SSPP dispersion law is recovered by enforcing the proper boundary conditions.

Due to the periodicity in the x -direction, in virtue of the Bloch theorem, it is sufficient to consider in detail the field distribution within the single period. Inside the grooves, E_z must vanish at the boundaries and thus we have

$$\begin{aligned} E_x &= s(y) \sum_{l \geq 0} P_z^{(l)} \cos \left[\frac{\pi l}{a} (x - x_L) \right] \\ &\quad \times \left(\alpha_+^{(l)} e^{i P_z^{(l)} z} + \alpha_-^{(l)} e^{-i P_z^{(l)} z} \right) \\ E_z &= -s(y) \sum_{l \geq 0} \frac{l\pi}{a} \sin \left[\frac{\pi l}{a} (x - x_L) \right] \\ &\quad \times \left(\alpha_+^{(l)} e^{i P_z^{(l)} z} - \alpha_-^{(l)} e^{-i P_z^{(l)} z} \right) \\ B_y &= s(y) \sum_{l \geq 0} \frac{P_z^{(l)2}}{\omega} \cos \left[\frac{\pi l}{a} (x - x_L) \right] \\ &\quad \times \left(\alpha_+^{(l)} e^{i P_z^{(l)} z} - \alpha_-^{(l)} e^{-i P_z^{(l)} z} \right) \end{aligned} \quad (1)$$

where l enumerates different modes, x_L is the x -coordinate of the left boundary of the groove, a is the width of the grooves, $s(y) = \sin[\pi(y - y_F)/w]$ describes the confinement of the EM field in the y -direction, $P_z^{(l)2} = (\frac{\omega}{c})^2 - (\frac{\pi}{w})^2 - (\frac{\pi l}{a})^2$ and $\alpha_+^{(l)}$ and $\alpha_-^{(l)}$ are the amplitudes of the waves propagating upward and downward, respectively.

Inside the arm due to the Bloch theorem, the components are given by

$$\begin{aligned} E_x &= s(y) \sum_m Q_z^{(m)} e^{i q_m x} \left(\beta_+^{(m)} e^{i Q_z^{(m)} z} + \beta_-^{(m)} e^{-i Q_z^{(m)} z} \right) \\ E_z &= -s(y) \sum_m q_m e^{i q_m x} \left(\beta_+^{(m)} e^{i Q_z^{(m)} z} - \beta_-^{(m)} e^{-i Q_z^{(m)} z} \right) \\ B_y &= s(y) \frac{P_z^2}{\omega} \sum_m e^{i q_m x} \left(\beta_+^{(m)} e^{i Q_z^{(m)} z} - \beta_-^{(m)} e^{-i Q_z^{(m)} z} \right) \end{aligned} \quad (2)$$

where $q_m = \beta + \frac{2\pi m}{d}$, β is the SSPP propagation constant, d is the period of the structure, $P_z = P_z^{(0)}$, and $Q_z^{(m)2} = P_z^2 - q_m^2$.

Let z_B be the coordinate of the groove–arm interface. Enforcing the continuity of E_x and B_y at the interface, one can find the relation between amplitudes $\alpha_{\pm}^{(l)}$ and $\beta_{\pm}^{(m)}$. The procedure is based on treating E_x in (1) and B_y in (2) as Fourier expansions of functions, which should take the specific form at $z = z_B$. For example, limiting expansions in (1) and (2) to the same number of terms, one finds $\beta_+^{(m)} e^{i Q_z^{(m)} z_B} + \beta_-^{(m)} e^{-i Q_z^{(m)} z_B}$ from the condition that E_x in (2) vanishes in the region $x < x_L$ and $x > x_L + a$. Further, $\alpha_+^{(l)} e^{i P_z^{(l)} z_B} - \alpha_-^{(l)} e^{-i P_z^{(l)} z_B}$ are found from the continuity of B_y . Solving the obtained system of equations with respect to $\beta_{\pm}^{(m)}$, one obtains the transfer matrix, which maps the state of the EM field inside the groove into the state of the field inside the arm. From the formal point of view, the requirement of the number of terms in (1) and (2) being the same ensures that the dimensions of the spaces of the states of the EM field in the groove and in the arm are the same. This can be avoided in waveguides with the corrugation along one

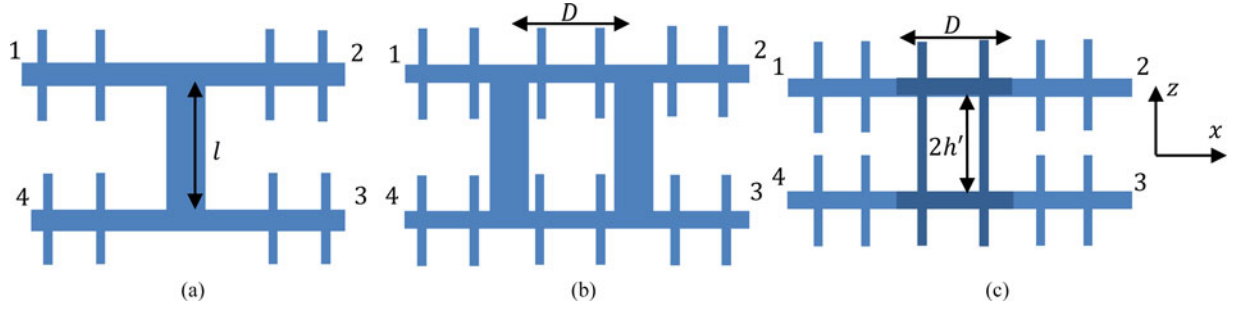


Fig. 2. Schematic view of analyzed designs of beam splitters. In the contra-propagating and co-propagating schemes, the input ports are 1, 2 and 1, 4, respectively. (a) Two waveguides with the distance $l = 230 \mu\text{m}$ between the arms are connected by the SC. (b) Arms are connected by TCs with the separation $D = 500 \mu\text{m}$ between them. (c) Arms are coupled by means of the two-arm waveguide with common grooves $h' = 100 \mu\text{m}$.

side only [28] or in highly symmetrical two-sided single-arm waveguides [21] but is necessary in the general case.

In order to make main formulas less cumbersome, we will keep only terms with $l = 0$ and $m = 0$ in (1) and (2), which is justified for analysis of the low frequency part of the spectrum. Incorporating phase factors $e^{\pm i Q_z z_B}$, where $Q_z = Q_z^{(0)}$, and $e^{\pm i P_z z_B}$ into the amplitudes α_{\pm} and β_{\pm} we find implementing the procedure outlined above the relation between vectors $|\alpha\rangle = (\alpha_+, \alpha_-)^T$ and $|\beta\rangle = (\beta_+, \beta_-)^T$ describing the EM field in the groove and in the arm, respectively, $|\beta\rangle = \hat{T}_{a,g}|\alpha\rangle$, where the transfer matrix through the groove–arm interface is

$$\hat{T}_{a,g} = \frac{ie^{-i\beta x_c}}{2SQ_z} \begin{pmatrix} t_1 + t_2 & t_1 - t_2 \\ t_1 - t_2 & t_1 + t_2 \end{pmatrix}. \quad (3)$$

Here, $x_c = x_L + \frac{a}{2}$ is the x -coordinate of the center of the groove, $S = \sqrt{a/d} \text{sinc}(\frac{\beta a}{2})$, $t_1 = S^2 P_z d$, and $t_2 = Q_z a$. The transfer matrix for the transition from the arm to the groove is found by simple inversion $\hat{T}_{g,a} = \hat{T}_{a,g}^{-1}$.

Since the phase factors were incorporated into the amplitudes, the phase difference between the amplitudes at opposite ends of an element (either groove or arm) is accounted for by introducing diagonal matrices $\hat{T}_{g,g} = \text{diag}(e^{i P_z h}, e^{-i P_z h})$ and $\hat{T}_{a,a} = \text{diag}(e^{2i Q_z t}, e^{-2i Q_z t})$ for the groove with height h and the arm with height $2t$.

The total transfer matrix \hat{T}_{tot} connecting the state of the EM field at the upper and lower ends of the structure is found by taking the ordered product of the transfer matrices through individual elements. For example, for the single-arm waveguide, this is,

$$\hat{T}_{SA} = \hat{T}_{gg} \hat{T}_{ga} \hat{T}_{aa} \hat{T}_{ag} \hat{T}_{gg} \quad (4)$$

while for the two-arm waveguide with shared grooves, we have

$$\hat{T}_{TA} = \hat{T}_{gg} \hat{T}_{ga} \hat{T}_{aa} \hat{T}_{ag'} \hat{T}_{g'g'} \hat{T}_{g'a} \hat{T}_{aa} \hat{T}_{ag} \hat{T}_{gg}. \quad (5)$$

The distribution of the field must satisfy certain boundary conditions at the ends of the structure. For the case of our main interest, when the structure is terminated by closed grooves, E_x must vanish at the ends. Thus, we have $\alpha_+ + \alpha_- = 0$ or in vector notations $x|\alpha\rangle = 0$ or equivalently $|\alpha\rangle = c|-x\rangle$, where c is an arbitrary number, $|\pm x\rangle \equiv (1, \pm 1)^T / \sqrt{2}$ and bra- and ket-vectors are related as usual through Hermitian conjugation.

Thus, in the case of our main interest, closed structures, the SSPP dispersion equations are

$$\langle x | \hat{T}_{\text{tot}} | -x \rangle = 0. \quad (6)$$

Since the left-hand side of this equation defines an analytic function of ω , for a given β , (6) holds only for isolated frequencies $\omega = \omega_i(\beta)$, which thus define branches of the SSPP dispersion curve when β varies from $-\pi/d$ to π/d .

Due to the mirror symmetry of the structures under consideration, the dispersion equation factorizes $D^{(e)}(\omega, \beta) D^{(o)}(\omega, \beta) = 0$ because the modes possess the definite transformation properties under reflections about the middle line. It is convenient to classify the modes according to the sign of charge on the horizontal boundaries, or, equivalently, according to the sign of E_z : the even and odd modes are characterized by even and odd functions $E_z(z)$. The even mode, therefore, has E_x vanishing at the middle line and thus the transfer matrix through half of the structure, \hat{T}_{half} , must map $|-x\rangle$ into $|-x\rangle$, which leads to

$$D^{(e)}(\omega, \beta) \equiv \langle x | \hat{T}_{\text{half}} | -x \rangle = 0. \quad (7)$$

The similar argument for an odd mode yields

$$D^{(o)}(\omega, \beta) \equiv \langle -x | \hat{T}_{\text{half}} | -x \rangle = 0. \quad (8)$$

For the single-arm waveguide, this leads to already known result

$$\begin{aligned} D_{SA}^{(e)}(\omega, \beta) &= 1 + \eta \frac{\tan(P_z h)}{\tan(Q_z t)} \\ D_{SA}^{(o)}(\omega, \beta) &= 1 - \eta \tan(P_z h) \tan(Q_z t) \end{aligned} \quad (9)$$

where $\eta = S^2 \frac{P_z}{Q_z}$. First three branches determined by (9) are shown in Fig. 3.

The dispersion law of SSPP in the two-arm waveguide with shared grooves is derived in the same way. It should be noted that in this case $D_{TA}^{(e)}(\omega, \beta) \equiv \langle x | \hat{T}_{\text{half}} | -x \rangle = 0$ has the form for the dispersion equation of the single-arm waveguide with grooves, generally, of different heights h and h' . The nonzero difference between them breaks the symmetry of the effective single-arm waveguide, which leads to the coupling between its even and odd modes. Thus, we have

$$D_{TA}^{(e)}(\omega, \beta) = D_{SA}^{(e)}(\omega, \beta) D_{SA}^{(o)}(\omega, \beta)$$

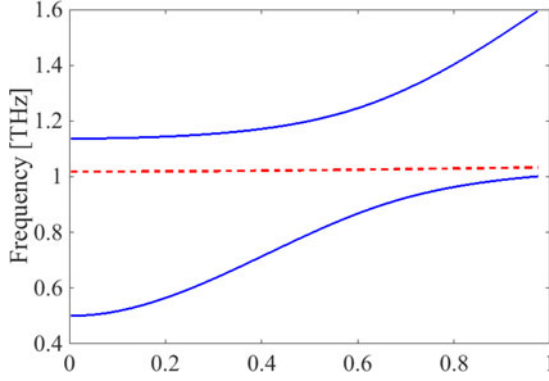


Fig. 3. Lowest three bands of SSPP in the single-arm waveguide (terminating parts of structures shown in Fig. 2). Solid lines show solutions of $D_{SA}^{(e)}(\omega, \beta) = 0$ and correspond to the first and second symmetric modes. The dashed line depicts the first antisymmetric mode and is found from $D_{SA}^{(o)}(\omega, \beta) = 0$.

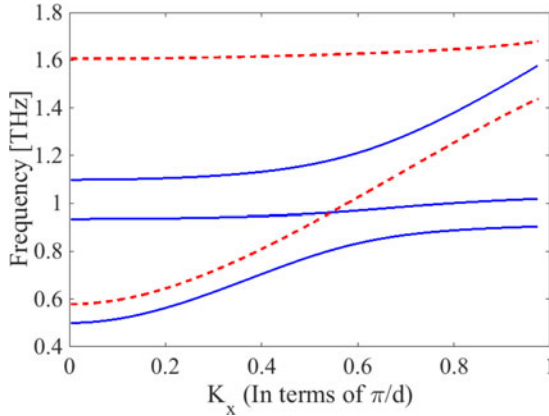


Fig. 4. SSPP dispersion law in the two-arm waveguide with shared grooves [the middle part of the structure shown in Fig. 2(c)]. Solid and dashed lines show symmetric and antisymmetric modes, respectively.

$$- (1 - \eta^2) \frac{\sin^2 \left[\frac{1}{2} (h - h') P_z \right]}{\cos^2 \left[\frac{1}{2} (h + h') P_z \right]} \quad (10)$$

which, in particular, shows the effect of the length of the shared grooves on the SSPP dispersion curves.

The two-arm waveguide, however, does not have the convenient factorization property and has somewhat cumbersome form

$$D_{TA}^{(o)}(\omega, \beta) = \cos [P_z (h + h')] - \tan (2Q_z t) [\eta \cos (P_z h) \times \sin (P_z h') + \eta^{-1} \sin (P_z h) \cos (P_z h')] \quad (11)$$

The solutions of equations $D_{TA}^{(e)}(\omega, \beta) = 0$ and $D_{TA}^{(o)}(\omega, \beta) = 0$ are shown in Fig. 4.

Obtained dispersion laws allow us to discuss the main features of the SSPP propagation through beam splitters. The easiest case is the implementation shown in Fig. 2(a), which we will refer to as the single-connector (SC) beam splitter. It can be regarded as consisting of two connected T-junctions. Thus, considering ports 1 and 2 as input ports and ports 3 and 4 as output, that

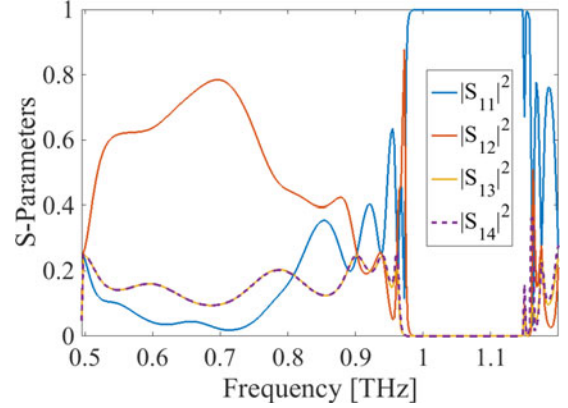


Fig. 5. Frequency dependence of S -parameters of the SC beam splitter.

is in the contra-propagating scheme, one can expect that due to the mirror symmetry with respect to the central vertical line the supplied input should be split equally between the output ports.

In order to characterize quantitatively the transport properties, we introduce $|S(i, j)|^2$, the normalized output power at port j with the input at port i , so that $|S(i, 1)|^2 + \dots + |S(i, 4)|^2 = 1$. In the contra-propagating setup, ports 1 and 2 (see Fig. 2) are input ports and ports 3 and 4 are regarded as output. In the co-propagating scheme, the input is supplied at ports 1 and 4 and the output is collected at ports 2 and 3. The characteristic of special importance, as will be illustrated in the next section, is the splitting ratio, or balance. For a symmetric contra-propagating beam splitter, i.e., with input ports 1 and 2, the balance is fully characterized by the ratio $b(\omega) = |S(1, 3)|^2 / |S(1, 4)|^2$, for the co-propagating beam splitter, when ports 1 and 4 are input, the splitting ratio is defined as $b(\omega) = |S(1, 2)|^2 / |S(1, 3)|^2$. For both cases, when $b(\omega) = 1$ the beam splitter is balanced; otherwise, it is unbalanced.

Fig. 5 shows the frequency dependence of the parameters $|S(i, j)|^2$ for the simplest design with one connector. It is assumed here and in the following figures that the input signal is supplied at port 1. Due to the symmetry of the structure, the full set of parameters $|S(i, j)|^2$ is obtained by simple re-enumeration of the ports. For example, for the contra-propagating scheme, the output signal with input at port 2 is found as $|S(2, 3)|^2 = |S(1, 4)|^2$ and $|S(2, 4)|^2 = |S(1, 3)|^2$, while the backscattered signal is found as $|S(2, 2)|^2 = |S(1, 1)|^2$ and $|S(2, 1)|^2 = |S(1, 2)|^2$. For the co-propagating scheme, the input is supplied at ports 1 and 4; hence, the output signal is determined by $|S(1, 2)|^2 = |S(4, 3)|^2$ and $|S(1, 3)|^2 = |S(4, 2)|^2$ and the backscattered signal is found from $|S(1, 1)|^2 = |S(4, 4)|^2$ and $|S(1, 4)|^2 = |S(4, 1)|^2$.

The characteristic feature of Fig. 5 is practically coinciding curves $|S(1, 3)|^2$ and $|S(1, 4)|^2$, which characterize the output signal in the contra-propagating scheme. This confirms the observation based on the symmetry of the structure made above. At the same time, it should be noticed that in the co-propagating scheme the equal splitting is reached when curves corresponding to $|S(1, 2)|^2$ and $|S(1, 3)|^2$ intersect, which occurs at isolated

frequencies near the low-frequency edge of the SSPP waveguide.

As has been discussed above, another important characteristic is the intensity of backscattering, which is defined in terms of the scattering intensities as $R = |S(1, 1)|^2 + |S(1, 2)|^2 = 1 - |S(1, 3)|^2 - |S(1, 4)|^2$. Fig. 5 demonstrates that for the SC design connector the high intensity of the backscattered signal $R(\omega) > 0.5$ is rather typical, which, as has been discussed above, may be a highly undesirable property. The numerical calculations were performed using HFSS simulation package [32], and the ports are terminated to the matched load, so that there is no reflection at the port's termination back into the structure.

The problem of significant backscattering can be approached utilizing more complex designs in two ways: with the help of destructive interference of backscattered waves or by reducing backscattering itself. The implementation of the first principle in the beam splitter with TCs is shown in Fig. 2(b).

In this case, the backscattered field at the input ports is the result of interference of waves scattered on different junctions. In order to get better understanding of the mechanism of reduction of backscattering, we consider the propagation across the beam splitter approximating the propagation of the EM wave into the connector by the main component with the propagation constant $k = \sqrt{P^2 - (\frac{\pi}{d_C})^2}$, where d_C is the width of the connector in the x -direction. Then, the propagation of the SSPP can be described by the transfer matrices of the form $T^{(e)} = T_C^{(e)} T_W T_C^{(e)}$ and $T^{(o)} = T_C^{(o)} T_W T_C^{(o)}$, for the even and odd modes of the beam splitter, respectively. The scattering into the even and odd modes of the connector is described by the transfer matrices [33]

$$T_C^{(e)} = \begin{pmatrix} 1 & 0 \\ iZ_1^{-1} \tan(kl/2) & 1 \end{pmatrix} \quad (12)$$

and

$$T_C^{(o)} = \begin{pmatrix} 1 & 0 \\ -iZ_1^{-1} \cot(kl/2) & 1 \end{pmatrix} \quad (13)$$

respectively, and the propagation of the SSPP in the arm is described by

$$T_W = \begin{pmatrix} \cos(\beta D) & i Z_0 \sin(\beta D) \\ -i Z_0 \sin(\beta D) & \cos(\beta D) \end{pmatrix}. \quad (14)$$

Here, D and l are the distances between the arms and connectors, respectively, $Z_1 = \omega/k$, $Z_0 = -\omega\beta/c^2 P^2$. Parameters $S(i, j)$ can be expressed in terms of the matrix elements of the transfer matrices $T^{(e)}$ and $T^{(o)}$ (see, e.g., [33, Sec. IV]). Imposing the condition of minimal power at the input ports, i.e., minimal backscattering, we find that the necessary condition is

$$\tan\left(\frac{kl}{2}\right) = 1. \quad (15)$$

Thus, one can achieve reduced backscattering in TC at given frequency by making the structure with specially chosen distance between the arms. In order to demonstrate this effect, we

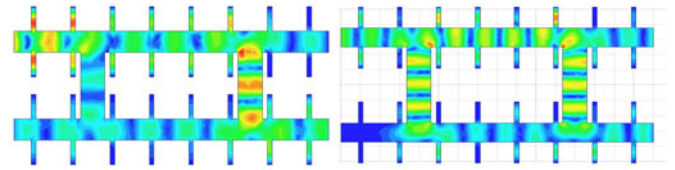


Fig. 6. Significant reduction of the intensity of backscattering in the TC beam splitter with variation of the distance between the arms. The input is supplied at port 1 and backscattering is registered at port 4.

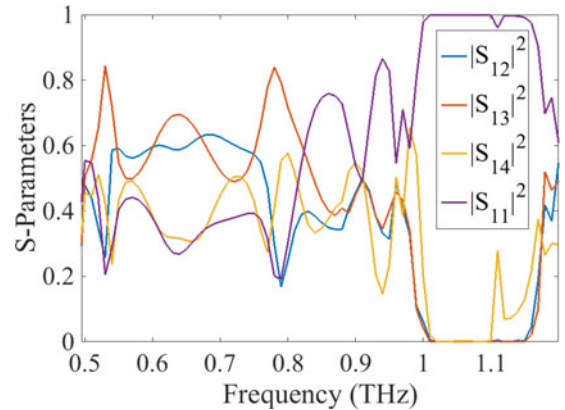


Fig. 7. Frequency dependence of S -parameters of the TC beam splitter.

compare in Fig. 6 the field distribution inside two structures with slightly different l at the same frequency.

The frequency dependence of the S -parameters of the TC is shown in Fig. 7. It should be noted that while backscattering in TC is significantly reduced comparing to SC, the simultaneous reach of balanced splitting and low backscattering requires careful adjusting the parameters of the structure and thus this design is more suitable for narrowband applications.

More direct control over backscattering is achieved in the implementation of the SSPP BS shown in Fig. 2(c). The advantage of such constructed beam splitter is that the translational symmetry is broken in a less invasive way. Moreover, by carefully choosing the characteristics of the waveguides, one can eliminate the variation of the SSPP propagation constant at the junction between the parts of the waveguide with disjoint arms and with arms sharing grooves thus reducing the backscattering in a stable (nonresonant) manner. Indeed, as (10) shows, the fundamental branch of a two-arm waveguide can be presented as a result of coupling between the even mode of the single-arm waveguide (i.e., its fundamental branch) and the lowest odd mode, with the coupling parameter proportional to the difference between heights of the shared and nonshared grooves. Thus, for frequencies not too close to the edge of the fundamental branch, where the coupling between the even and odd modes is significant, the lowest modes of the single- and two-arm waveguides differ only slightly. Therefore, for a given frequency, the mismatch between the propagation constants, and, hence, the impedance mismatch, between the parts of the beam splitter with disjoint arms and with arms sharing grooves, is small. This observation is confirmed by the numerical simula-

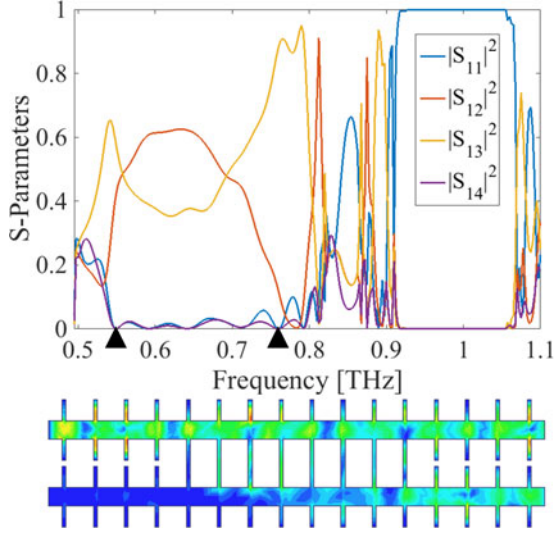


Fig. 8. (Upper panel) S -parameters of the beam splitter based on coupling through shared grooves. The black markers indicate the frequency range with suppressed backscattering. (Lower panel) The field distribution inside the beam splitter demonstrating the reduced back scattering and the gradual formation of the split signal.

tions presented in Fig. 8. It shows in particular that, as well as in the case of the beam splitter with TCs, the equal splitting ratio is reached at isolated frequencies. A drawback of this design, however, should be noted. The coupling between SSPP modes propagating in different arms is relatively weak. This results in the necessity of having long length of the beam splitter, when the effect of attenuation may become pronounced.

III. FOUR-TERMINAL BEAM SPLITTER WITH BACKSCATTERING

One of the important applications of the beam splitter is in various quantum optical experiments, for instance, Hong–Ou–Mandel type of experiments and homodyne detection. The standard description of these experiments assumes that the distinction between the input and output ports is strict. At the same time, all designs considered in the previous section demonstrate backscattering for a generic frequency. As a result, the standard description of the beam splitter adopted in quantum optics is not directly applicable but requires a slight generalization to account that sending a pulse into either port produces, generally speaking, outgoing signals in all port. Thus, the relation between incoming and outgoing states is provided by a 4×4 scattering matrix \hat{S}

$$\begin{pmatrix} b_1 \\ \vdots \\ b_4 \end{pmatrix} = \hat{S} \begin{pmatrix} a_1 \\ \vdots \\ a_4 \end{pmatrix} \quad (16)$$

where a_i is the operator corresponding to incoming SSPP in port i and b_i describe outgoing SSPP.

Out of the variety of possible applications of transformations of quantum states described by (16), we pay the special attention to the implementation of the balanced homodyne detection scheme. Without the loss of generality, we can consider the case

when the incoming SSPP states are supplied in ports 1 and 2 only, while only the outgoing states in ports 3 and 4 are detected.

In order to explicate such setup, we collect indices $\{1, 2\}$ into set in and indices $\{3, 4\}$ into set out . Then, (16) can be rewritten in the block form

$$\begin{pmatrix} \mathbf{b}_{in} \\ \mathbf{b}_{out} \end{pmatrix} = \hat{S} \begin{pmatrix} \mathbf{a}_{in} \\ \mathbf{a}_{out} \end{pmatrix} \quad (17)$$

where the scattering matrix \hat{S} is written as

$$\hat{S} = \begin{pmatrix} \hat{S}_{in,in} & \hat{S}_{in,out} \\ \hat{S}_{out,in} & \hat{S}_{out,out} \end{pmatrix}$$

and $\hat{S}_{I,J}$ are 2×2 matrices.

A general one-particle observable involving ports 3 and 4 can be represented as operator

$$V_{out} = v_0 J_0(\mathbf{b}_{out}^+, \mathbf{b}_{out}) + \mathbf{v} \cdot \mathbf{J}(\mathbf{b}_{out}^+, \mathbf{b}_{out}) \quad (18)$$

where a scalar v_0 and a 3-D unit vector \mathbf{v} characterize measured quantity and

$$J_i(\mathbf{b}^+, \mathbf{b}) = \frac{1}{2} \sum_{m,n \in \{3,4\}} b_m^+(\sigma_i)_{m,n} b_n \quad (19)$$

with $\sigma_0 = \hat{1}/2$ and σ_i being the usual Pauli matrices.

It should be noted that the similar approach can be used for describing a general observable involving all four ports. In this case, instead of the Pauli matrices, one needs to employ the full family of generators of $su(4)$ Lie algebra. This general case, however, is beyond the scope of the current consideration and will not be analyzed here.

Equation (18) presents the observable on the basis of the outgoing states. Using (17) and taking into account that we are only interested in the case when the input is supplied at ports 1 and 2, we find

$$V_{in} = v'_0 J_0(\mathbf{a}_{in}^+, \mathbf{a}_{in}) + \mathbf{v}' \cdot \mathbf{J}(\mathbf{a}_{in}^+, \mathbf{a}_{in}) \quad (20)$$

where we have introduced the modified pair (v'_0, \mathbf{v}') defined by the relation

$$\sum_i v'_i \sigma_i = \sum_i v_i \left(\hat{S}_{out,in}^+ \sigma_i \hat{S}_{out,in} \right). \quad (21)$$

This relation can be alternatively written in terms of linear transformation $v'_i = \sum_j R_{i,j} v_j$, where the matrix elements $R_{i,j}$ are found using the orthonormality relation $\text{Tr}(\sigma_i \sigma_j) = 2^{-1} \delta_{i,j}$. The application of this formalism for the homodyne detection is simplified by two circumstances. First, we require that the measured quantity must be a linear function of the operators corresponding to the unknown state (say, supplied at port 1). Thus, we require that $v'_0 = v'_z = 0$. Second, we take into consideration that only intensity is measured at the output ports, so that $v_x = v_y = 0$. Applying the orthonormality relation, these conditions can be written as a system of homogeneous equations with respect to v_0 and v_z

$$\text{Tr} \left[\sigma_i \hat{S}_{out,in}^+ (v_0 \sigma_0 + v_z \sigma_z) \hat{S}_{out,in} \right] = 0 \quad (22)$$

where $i = 0, z$. Writing out explicitly the matrices involved, one finds that this system has a nontrivial solution $v_0 = 0, v_z =$

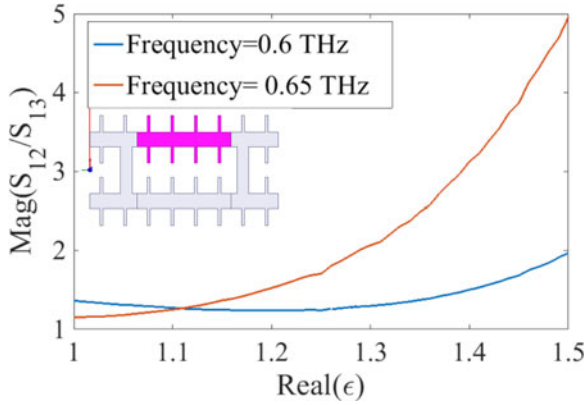


Fig. 9. Change of the splitting ratio at two close frequencies in a tunable beam splitter with the variation of the dielectric constant of the filling dielectric. The inset shows the simulated structure.

1 only when $|S_{3,1}|^2|S_{4,2}|^2 = |S_{4,1}|^2|S_{3,2}|^2$. For the case of a design symmetric with respect to the middle line, this implies that in order to be employed in the homodyne detection scheme the beam splitter must be balanced, so that $|S_{3,1}|^2 = |S_{4,2}|^2 = |S_{4,1}|^2 = |S_{3,2}|^2 = p$. Using these findings in (21), we find

$$\begin{aligned} v'_x &= p(\cos(\phi_{3,1} - \phi_{3,2}) - \cos(\phi_{4,1} - \phi_{4,2})) \\ v'_y &= p(\sin(\phi_{3,1} - \phi_{3,2}) - \sin(\phi_{4,1} - \phi_{4,2})) \end{aligned} \quad (23)$$

where $\phi_{i,j} = \arg(S_{i,j})$ are phases of the respective scattering amplitudes. Equation (23) shows the important consequence of the symmetry of the beam splitter on the form of the observable operator on the basis of incoming states. In this case, one has $\phi_{3,1} - \phi_{3,2} = \phi_{4,2} - \phi_{4,1}$ and, as a result, $v'_x \equiv 0$. Thus, the beam splitters with the symmetry with respect to the middle line allow one to measure only the p -quadrature.

By breaking the mirror symmetry, for instance, by means of filling the beam splitter partially by a dielectric material, as is considered in the next section, the phase parameter of the beam splitter can be varied. Such modification, however, leads in general to changing the splitting ratio and, as a result, the beam splitter becomes unbalanced. Thus, the variation of the phase parameter requires more complex control schemes, which are not considered here.

IV. TUNABLE BEAM SPLITTER

The propagation of the SSPP inside the beam splitter as in the implementations with TCs and with shared grooves provides an opportunity for a flexible control over the SSPP flow. In order to demonstrate these properties, we consider the beam splitter with TCs with the upper arm filled with a dielectric. The variation of the dielectric constant leads to changing the splitting ratio as is shown in Fig. 9.

V. CONCLUSION

We have analyzed the basic designs of beam splitters for SSPP. The main attention was paid to two important characteristics: splitting ratio and the intensity of back scattering. We show that

from the perspective of balanced splitting, the simplest design—two connected SSPP waveguides in contra-propagating setup—provides the best solution. This beam splitter demonstrates near equal splitting for all frequencies except inside SSPP band gaps. At the same time, it demonstrates high intensity backscattering, which poses a certain problem for applications in large-scale optical setups. We show that sacrificing the property of broadband balance, the intensity of backscattering can be reduced employing more complex designs by means of destructive interference of the backscattered signal (in the design with TCs) or reducing scattering by minimizing the mismatch of the SSPP propagation constant (the design with shared grooves).

The implementations of the beam splitters were analyzed from the perspective of their applications in quantum optical setups using the homodyne detection scheme as an example. We extend the standard description of the beam splitter in order to incorporate the inevitable backscattering and show that the only parameter of importance is the splitting ratio.

Finally, we demonstrate the filtering properties of the SSPP beam splitter by considering the variation of the splitting ratio of the beam splitter with changing the dielectric constant of the material filling one arm.

REFERENCES

- [1] S. Koenig *et al.*, “Wireless sub-THz communication system with high data rate,” *Nature Photon.*, vol. 7, pp. 977–981, 2013.
- [2] T. Kürmer and S. Priebe, “Towards THz communications—Status in research, standardization and regulation,” *J. Infrared Millim. THz Waves*, vol. 35, pp. 53–62, 2014.
- [3] M. Tonouchi, “Cutting-edge terahertz technology,” *Nature Photon.*, vol. 1, pp. 97–105, 2007.
- [4] T. Nagatsuma, “Terahertz technologies: Present and future,” *IEICE Electron. Exp.*, vol. 8, pp. 1127–1142, 2011.
- [5] Y. Yuan, J. He, J. Liu, and J. Yao, “Electrically controlled broadband THz switch based on liquid-crystal-filled multi-layer metallic grating structures,” *J. Phys. Conf. Series*, vol. 276, pp. 1742–6596, 2011.
- [6] M. Mittendorff *et al.*, “Ultrafast graphene-based broadband THz detector,” *Appl. Phys. Lett.*, vol. 103, 2013, Art. no. 021113.
- [7] K. Peng *et al.*, “Single nanowire photoconductive terahertz detectors,” *Nano Lett.*, vol. 15, pp. 206–210, 2015.
- [8] G. P. Williams, “Filling the THz gap—high power sources and applications,” *Rep. Prog. Phys.*, vol. 69, pp. 301–326, 2006.
- [9] M. Feiginov, C. Sydlo, O. Cojocari, and P. Meissner, “Resonant-tunnelling-diode oscillators operating at frequencies above 1.1 THz,” *Appl. Phys. Lett.*, vol. 99, 2011, Art. no. 233506.
- [10] P. Mukherjee and B. Gupta, “Terahertz (THz) frequency sources and antennas—A brief review,” *Int. J. Infrared Millim. Waves*, vol. 29, pp. 1091–1102, 2008.
- [11] G. Gallot, S. P. Jamison, R. W. McGowan, and D. Grischkowsky, “Terahertz waveguides,” *J. Opt. Soc. Amer. B, Opt. Phys.*, vol. 17, pp. 851–863, 2000.
- [12] R. W. McGowan, G. Gallot, and D. Grischkowsky, “Propagation of ultrawideband short pulses of terahertz radiation through submillimeter diameter circular waveguides,” *Opt. Lett.*, vol. 24, pp. 1431–1433, 1999.
- [13] L.-J. Chen, H.-W. Chen, T.-F. Kao, J.-Y. Lu, and C.-K. Sun, “Low-loss subwavelength plastic fiber for terahertz waveguiding,” *Opt. Lett.*, vol. 31, pp. 308–310, 2006.
- [14] R. Mendis and D. Grischkowsky, “Plastic ribbon THz waveguides,” *J. Appl. Phys.*, vol. 88, pp. 4449–4451, 2000.
- [15] A. Dupuis, K. Stoeffler, B. Ung, C. Dubois, and M. Skorobogatii, “THz transmission measurements of hollow-core bragg fibers,” *J. Opt. Soc. Amer. B, Opt. Phys.*, vol. 28, pp. 896–907, 2011.
- [16] T. Ito, Y. Matsuura, M. Miyagi, H. Minamide, and H. Ito, “Flexible terahertz fiber optics with low bend-induced losses,” *J. Opt. Soc. Amer. B, Opt. Phys.*, vol. 24, pp. 1230–1235, 2007.

- [17] N. Talebi and M. Shahabadi, "Spoof surface plasmons propagating along a periodically corrugated coaxial waveguide," *J. Phys. D, Appl. Phys.*, vol. 43, 2010, Art. no. 135302.
- [18] K. Wang and D. M. Mittleman, "Metal wires for terahertz wave guiding," *Nature*, vol. 432, pp. 376–379, 2004.
- [19] J. B. Pendry, L. Martín-Moreno, and F. J. García-Vidal, "Mimicking surface plasmons with structured surfaces," *Science*, vol. 305, pp. 847–848, 2004.
- [20] M. Aghadjani and P. Mazumder, "THz polarizer controller based on cylindrical spoof surface plasmon polariton (C-SSPP)," *IEEE Trans. THz. Sci. Technol.*, vol. 5, no. 4, pp. 556–563, Jul. 2015.
- [21] Z. Xu, K. Song, and P. Mazumder, "Analysis of doubly corrugated spoof surface plasmon polariton (DC-SSPP) structure with sub-wavelength transmission at THz frequencies," *IEEE Trans. THz. Sci. Technol.*, vol. 2, no. 3, pp. 345–354, May 2012.
- [22] S. A. Maier, S. R. Andrews, L. Martín-Moreno, and F. J. García-Vidal, "Terahertz surface plasmon-polariton propagation and focusing on periodically corrugated metal wires," *Phys. Rev. Lett.*, vol. 97, 2006, Art. no. 176805.
- [23] M. Aghadjani and P. Mazumder, "Terahertz switch based on waveguide-cavity-waveguide comprising cylindrical spoof surface plasmon polariton," *IEEE Trans. Electron Devices*, vol. 62, no. 4, pp. 1312–1318, Apr. 2015.
- [24] M. Barangi, M. Aghadjani, and P. Mazumder, "Design and analysis of a terahertz SSPP switch using piezoelectric materials," in *Proc. IEEE 15th Int. Conf. Nanotechnol.*, Rome, Italy, 2015, pp. 678–681.
- [25] K. Song and P. Mazumder, "Active terahertz spoof surface plasmon polariton switch comprising the perfect conductor metamaterial," *IEEE Trans. Electron Devices*, vol. 56, no. 11, pp. 2792–2799, Oct. 2009.
- [26] K. Song and P. Mazumder, "Dynamic terahertz spoof surface plasmon-polariton switch based on resonance and absorption," *IEEE Trans. Electron Devices*, vol. 58, no. 7, pp. 2172–2176, Jul. 2011.
- [27] X. Zhao and P. Mazumder, "Terahertz beam steering with doped GaAs phase modulator and a design of spatial-resolved high-speed terahertz analog-to-digital converter," *IEEE Trans. Electron Devices*, vol. 61, no. 6, pp. 2195–2202, Jun. 2014.
- [28] B. D. Mcvey, M. A. Basten, J. H. Booske, J. Joe, and J. E. Scharer, "Analysis of rectangular waveguide-gratings for amplifier applications," *IEEE Trans. Microw. Theory Techn.*, vol. 42, no. 6, pp. 995–1003, Jun. 1994.
- [29] C. C. Homes, G. L. Carr, R. P. S. M. Lobo, J. D. LaVeigne, and D. B. Tanner, "Silicon beam splitter for far-infrared and terahertz spectroscopy," *Appl. Opt.*, vol. 46, pp. 7884–7888, 2007.
- [30] C. W. Berry and M. Jarrahi, "Broadband terahertz polarizing beam splitter on a polymer substrate," *J. Infrared Millim. THz Waves*, vol. 33, pp. 127–130, 2012.
- [31] T. Niu *et al.*, "Terahertz reflectarray as a polarizing beam splitter," *Opt. Exp.*, vol. 22, pp. 16148–16160, 2014.
- [32] *Ansoft HFSS*, Ansys Inc., Pittsburgh, PA, USA, 2013.
- [33] D. M. Pozar, *Microwave Engineering*, 3rd ed. New York, NY, USA: Wiley, 2004.



Mahdi Aghadjani received the B.S. degree in electrical engineering from the Iran University of Science and Technology, Tehran, Iran, and the M.S. degree in electrical engineering from the University of Tehran, Tehran. He is currently working toward the Ph.D. degree as a Graduate Student Research Assistant at the Department of Electrical Engineering and Computer Science, University of Michigan, Ann Arbor, MI, USA.

His current research interests include designing optical and terahertz devices.



Mikhail Erementchouk received the Ph.D. degree in physics from the City University of New York, New York, NY, USA, in 2005.

He is currently a Visiting Researcher with the Department of Electrical Engineering and Computer Science, University of Michigan, Ann Arbor, MI, USA. His current research interests include quantum and classical optics, optical response of semiconductors, and transport in complex media.



Pinaki Mazumder (S'84–M'87–SM'95–F'99) received the Ph.D. degree from the University of Illinois at Urbana–Champaign, Urbana, IL, USA, in 1988.

He was the Lead Program Director with the Emerging Models and Technologies Program, University of Michigan, Ann Arbor, MI, USA, through the U.S. National Science Foundation. He has served in industrial research and development centers including AT&T Bell Laboratories, Murray Hill, NJ, USA, where he started the CONES Project called the first C modeling-based very large scale integration

(VLSI) synthesis tool, and Bharat Electronics Ltd., Bangalore, India, in 1985, where he had developed several high-speed and high-voltage analog-integrated circuits intended for consumer electronics products. He is currently a Professor with the Department of Electrical Engineering and Computer Science, University of Michigan. He has authored more than 200 technical papers and 4 books on various aspects of VLSI research works. His current research interests include current problems in nanoscale CMOS VLSI design, CAD tools, and circuit designs for emerging technologies, including quantum MOS and resonant tunneling devices, semiconductor memory systems, and physical synthesis of VLSI chips.

Dr. Mazumder is a Fellow of the American Association for the Advancement of Science (2008). He received the Digital's Incentives for Excellence Award, BF Goodrich National Collegiate Invention Award, and Defense Advanced Research Projects Agency Research Excellence Award.